INL/RPT-23-75169

Coupling Thermal-Hydraulics with Reactor Pressure Vessel Fracture Models

September 2023

Benjamin W. Spencer[1]
William M. Hoffman[1]
Albert Dahal[1]

[1]Idaho National Laboratory

INL is a U.S. Department of Energy National Laboratory
operated by Batelle Energy Alliance, LLC

INL/RPT-23-75169

Coupling Thermal-Hydraulics with Reactor Pressure Vessel Fracture Models

Benjamin W. Spencer[1]
William M. Hoffman[1]
Albert Dahal[1]

[1]**Idaho National Laboratory**

September 2023

Idaho National Laboratory
Computational Mechanics and Materials
Idaho Falls, Idaho 83415

http://www.inl.gov

Prepared for the
U.S. Department of Energy
Office of Nuclear Energy
Under DOE Idaho Operations Office
Contract DE-AC07-05ID14517

Page intentionally left blank

ABSTRACT

Because of the importance of maintaining the integrity of the reactor pressure vessel (RPV) in light-water reactors, significant effort has been devoted over the last several decades to understand the potential failure mechanisms, characterize how material properties evolve due to environmental conditions, and develop tools to assess the probability of fracture in aged RPVs during potential transient events. One important aspect of this problem that has not yet been fully addressed is the effects of nonuniform cooling on the RPV inner wall due to the way low-temperature water injected into the primary coolant system is distributed within the RPV during potential loss-of-coolant accident transients. Colder temperatures are expected in the regions near the inlets, causing a "cold-plume" effect. Rapid cooling of the RPV wall increases the likelihood of fracture initiation, and localized cooling due to cold-plume effects could potentially exacerbate this problem. The Grizzly code can perform a three-dimensional simulation of the RPV thermomechanical response as well as the probabilistic assessment of fracture for a population of pre-existing flaws, which is necessary to account for spatial variations in coolant temperature. This report documents a first effort to couple Grizzly RPV fracture models with computational fluid dynamics models performed using the Cardinal code, which allows for a realistic representation of the temperature distribution. This report demonstrates this coupling approach on two test cases: a simplified proof-of-concept scenario and a realistic small-break loss-of-coolant accident scenario. In both cases, the effects of the spatially varying temperature are evident; although, because the small-break loss-of-coolant accident scenario was far from challenging the RPV's margins, it is still inconclusive how important cold-plume effects are in realistic accident scenarios. However, this effort represents an important step toward performing realistic analyses to determine to what extent spatially nonuniform cooling might affect RPV integrity under more aggressive accident scenarios.

ACKNOWLEDGMENTS

The support of our colleagues at Argonne National Laboratory (Yiqi Yu and Dillon Shaver) and Penn State University (Elia Merzari) in developing computational fluid dynamics models used in this work was critical for the successful completion of this effort. Their work is documented in a separate report referenced herein.

This work was supported by the U.S. Department of Energy's Nuclear Energy Advanced Modeling and Simulation (NEAMS) program. This research utilized the resources of the High Performance Computing Center at Idaho National Laboratory, which is supported by the Office of Nuclear Energy of the U.S. Department of Energy and the Nuclear Science User Facilities under contract no. DE-AC07-05ID14517. This manuscript was authored by Battelle Energy Alliance, LLC under contract no. DE-AC07-05ID14517 with the U.S. Department of Energy. The U.S. Government retains a nonexclusive, paid-up, irrevocable, worldwide license to publish or reproduce the published form of this manuscript, or allow others to do so, for U.S. Government purposes.

CONTENTS

FIGURES

TABLES

1 INTRODUCTION

Light-water reactors (LWRs) currently supply the vast majority of commercial nuclear power worldwide and are the only operating type of nuclear reactor for commercial power generation in the United States. These reactors employ massive reactor pressure vessels (RPVs) to contain the reactor and serve as a first barrier against the release of material from the primary coolant system to the environment. RPVs are subjected to challenging environments, being exposed to approximately 300 °C coolant and high neutron flux, especially in the regions immediately adjacent to the reactor core. Long-term exposure to these conditions is well-known to embrittle the steel alloys that these RPVs are constructed from. Because of the essential role that RPVs fill in ensuring the safe operation of LWRs and the extreme difficulty in replacing or refurbishing an aged RPV, the ability to accurately characterize the risk of fracture in an RPV is essential for managing the currently operating LWRs.

To assess RPV integrity under transient conditions, an approach known as probabilistic fracture mechanics (PFM) has been developed by researchers internationally over decades. Specific details on these approaches vary among the researchers and software used, but these generally involve first performing a system-level thermal-hydraulic analysis to obtain histories of temperature and pressure that are applied to a thermomechanical RPV model, which is then used in detailed fracture-mechanics assessments of individual flaws in the RPV metal. A potentially significant issue with the methodology currently in widespread use is the assumption that temperatures and pressures in the RPV are spatially uniform. During most loss-of-coolant accident (LOCA) scenarios, lower-temperature coolant is injected into the primary coolant system, with regions near the inlet being cooled more rapidly than other regions of the RPV. The assumptions of uniform cooling are potentially not conservative, and higher-fidelity three dimensional (3D) models are essential for more realistically performing this type of simulation.

The tools developed under the U.S. Department of Energy's Nuclear Energy Advanced Modeling and Simulation (NEAMS) program are particularly well-suited to account for spatial variations in the temperatures in PFM simulations of an RPV under transient conditions. The Cardinal code supported by the NEAMS program enables coupling the NekRS high-fidelity computational fluid dynamics (CFD) code and the Multiphysics Object-Oriented Simulation Environment (MOOSE). This allows for 3D simulations that solve for fluid flow and heat transfer within the fluid to be coupled with MOOSE-based models for the RPV thermal response. The MOOSE-based Grizzly code, also supported by NEAMS, offers a unique capability to solve for the thermo-mechanical RPV response in 3D and performs PFM of sampled populations of flaws using the 3D RPV model response.

This report demonstrates the use of Cardinal and Grizzly for coupled PFM simulations that employ CFD to obtain temporally and spatially varying temperatures on the inner surface of the RPV and determine the probability of fracture initiation for a population of flaws with Grizzly, using those inner-wall surface temperatures from Cardinal. To our knowledge, this is a first-of-its-kind demonstration of such a capability and represents an important advance in the ability to accurately assess the safety of an embrittled RPV accounting for the effects of material aging and the complex thermal conditions under LOCA transients.

2 REACTOR PRESSURE VESSEL FRACTURE MODELING AND PLUME EFFECTS

Significant prior research has addressed RPV steel embrittlement and methods for assessing fracture under thermal-shock conditions [2]. Here we provide a brief summary of the phenomena leading to potential RPV fracture, methodologies commonly used in practice for PFM, and prior work on PFM assessments accounting for cold-plume effects.

RPVs generally contain many flaws introduced during the manufacturing process. Most of these have minimal safety consequences. However, transient loading conditions could result in a combination of high stresses and low temperatures that can result in fracture initiation at some of those flaws. Rapid temperature changes can cause significant thermal gradients, which can further increase the tensile stresses beyond those that might already be present due to internal pressurization. RPV steel becomes more brittle at lower temperatures, so transients involving rapid cooling are of particular concern because of the potential combination of low temperature and elevated stress in the material.

The methodologies in current practice for PFM of embrittled LWR RPVs under transient conditions generally include:

1. Performing a thermal-hydraulic analysis to obtain the temperature and pressure histories in the RPV
2. Simulating the thermomechanical response of the RPV under those temperature and pressure histories
3. Randomly sampling plausible populations of flaws
4. Using fracture mechanics models to evaluate the stress intensity factor (SIF) at each flaw location
5. Computing the embrittlement at each flaw location
6. Computing the probability of fracture for each flaw as a function of its SIF, temperature and embrittlement
7. Computing an aggregate probability of fracture for the RPV for a given RPV under the transient considered.

As described in a survey paper by Qian and Niffeneger [3], there are a number of codes used in practice for PFM assessments. Of those codes, PASCAL [4] and FAVOR [5] are the most widely used in practice, and generally represent state-of-the-art codes.

An important assumption made in the current state-of-the art PFM codes is that the temperatures experienced on the inner wall of the RPV during transient events are spatially uniform. Under this assumption, the RPV behavior can be represented as an infinite cylinder, and a 1D axisymmetric model can be used to simulate its thermomechanical response. This assumption is consistent with that of the reduced-order, system-level thermal-hydraulic codes used to provide transient temperatures.

These assumptions of uniform temperature have the important implication that they neglect the "cold-plume" effect, in which there are regions of lower-temperature coolant near the inlets than in the rest of the vessel. Physical modeling of this effect requires the use of 3D CFD models for the coolant behavior coupled with 3D models of the RPV thermomechanical response. Multiple efforts to perform this type of analysis have been published in recent years [6–8]. These studies all employed 3D CFD simulations coupled with 3D thermomechanical RPV models, and performed probabilistic analyses of specific selected flaws. Importantly, they did not consider the entire flaw population in the way that codes such as FAVOR or PASCAL can do (assuming spatially uniform behavior). Grizzly's capabilities for PFM analysis were previously demonstrated

in Reference [9], but using a contrived temperature distribution rather than one derived from CFD modeling. The present effort builds on that prior work by accounting for spatially nonuniform temperature effects from CFD modeling on full probabilistically sampled flaw populations.

3 APPROACH FOR PROBABILISTIC FRACTURE MECHANICS MODELING EMPLOYED IN THIS STUDY

Here we summarize the approach taken in the present study to couple 3D CFD models with 3D PFM models to capture the effects of nonuniform cooling on the probability of fracture initiation using the Grizzly and Cardinal codes. We first provide a summary of the implementation of PFM in Grizzly, followed by a description of the process used to transfer CFD solutions from Cardinal to Grizzly.

3.1 Grizzly Implementation of Probabilistic Fracture Mechanics

Grizzly's PFM algorithms generally follow the approach used by FAVOR [5], but these algorithms are adapted to allow their use in more general conditions. Notable unique features of Grizzly are its ability to use either 1D, 2D, or 3D representations of the global thermomechanical response of the RPV and use that in the PFM simulation, ability to use 3D fluence distributions read directly from data provided by a neutron-transport code [10], and ability to run PFM simulations in parallel to accelerate their execution. The main elements of the Grizzly simulation are summarized here. More detailed descriptions of Grizzly's algorithms for PFM are provided in Reference [9].

Prior to running PFM analysis, the global thermomechanical response of the RPV must be computed. This is done in Grizzly by using models provided by the TensorMechanics and HeatConduction modules, using the dimensionality necessary to capture the important features of the model response. The cladding and base metal are both represented in the model, with appropriate temperature-dependent properties. Once the global response is computed, Grizzly samples stresses and temperatures at points through the RPV wall thickness to provide coefficients for polynomial fits defining the variation of those quantities as a function of depth in the RPV wall. These fits are performed on a regular grid in the azimuthal and axial coordinates of a cylindrical coordinate system, as applicable depending on the dimensionality of the global model.

Once the global model response is calculated and the polynomial coefficients are obtained from it, the PFM assessment is performed in a separate analysis stage. The first step in the PFM analysis is to generate a set of random realizations of the population of flaws using Monte Carlo sampling based on specified distributions of flaws in each RPV. Values for the geometric dimensions (size, position, orientation, and aspect ratio), as well as parameters defining the local chemistry (concentrations of Cu, Ni, Mn, and P) and the nil-ductility reference temperature, RT_{NDT} are sampled for each flaw in an RPV realization. Each set of flaws for a single RPV is known as an RPV realization, and a sufficiently large number of RPV realizations must be generated to obtain converged solutions for the quantities of interest from the PFM analysis. The primary quantity of interest from the PFM analysis is the average value of the conditional probability of fracture initiation (CPI), which is the probability that a fracture will initiate at any of the flaws present in the RPV at each time step during the transient, given occurrence of the transient. Computing the CPI for the full vessel requires first computing CPI for each flaw.

Once the samples defining the flaw population are generated, the probability of fracture initiation at each flaw is computed. This entails computing the local material properties and driving forces for fracture. The material is characterized by a lower-bound toughness curve that is a function of the relative temperature (defined current temperature minus RT_{NDT}). Material embrittlement due to irradiation is assumed to be manifested as a shift in RT_{NDT}, following the semiempirical model of [11]. Because the neutron fluence and local temperature vary, these properties are computed for each sampled flaw.

In addition to the local toughness and temperature, K_I is needed for each flaw. To enable evaluating K_I for each of the sampled flaws with minimal computational effort, the weight function approach [12] is used, in

which K_I is expressed as a linear superposition of contributions from individual components of a polynomial expansion of the far-field stress as a function of through-wall position. The through-wall variation of the stress component normal to the flaw σ as a function of the depth a' relative to the flaw depth a is described by an n^{th}-order polynomial:

$$\sigma\left(\frac{a'}{a}\right) = C_0 + C_1\left(\frac{a'}{a}\right) + \cdots + C_n\left(\frac{a'}{a}\right)^n \tag{1}$$

where C_i are the polynomial coefficients of the stress distribution. K_I is computed as:

$$K_I = \sum_{i=0}^{n} C_i K_i \sqrt{\pi a} \tag{2}$$

where K_i are stress intensity factor influence coefficients (SIFICs).

Each SIFIC K_i is computed for a specific flaw geometry by evaluating K_I under far-field stresses corresponding to each term of the expansion of Equation 1 with all polynomial coefficients set to 0 except for C_i. This approach is adopted by the American Society of Mechanical Engineers (ASME) Boiler & Pressure Vessel Code, which provides closed-form expressions or tables for computing SIFICs for surface-breaking and subsurface (embedded) elliptical flaws in Section XI, Article A-3000 [13]. These solutions in the ASME code have evolved over the years, and the method used for embedded flaws here is based on the technique in Reference [14] to compute coefficients, which is used in the 2013 and earlier versions of the ASME code. The values of the stress coefficients for a specific flaw are interpolated from values at the corners of the cell of the grid in the azimuthal and axial coordinates on the RPV wall that contains that flaw.

Following the computation of K_I, a Weibull statistical model is used to compute the CPI of each flaw. A standard Weibull distribution is used to describe CPI as a function of K_I at the current relative temperature. Figure 1 shows a contour plot of CPI as a function of K_I and relative temperature. Once the CPI is computed for each flaw, the aggregate conditional probability of fracture initiation for any flaw in the RPV, $\mathrm{CPI_{RPV}}$, is computed as:

$$\mathrm{CPI_{RPV}} = 1 - \prod_{i=1}^{n_{\mathrm{flaw}}} (1 - \mathrm{CPI}_i) \tag{3}$$

where n_{flaw} is the number of flaws in the RPV and CPI_i is the maximum CPI for flaw i during that transient.

The aggregate $\mathrm{CPI_{RPV}}$ computed in Equation 3 is the CPI for a single realization of the flaw population. There is typically a small number of flaws in a given population with nonzero CPI values and significant variation in the $\mathrm{CPI_{RPV}}$ value between RPV realizations. The primary quantity of interest in a PFM calculation is the mean value of $\mathrm{CPI_{RPV}}$ over a series of Monte Carlo iterations. For these Monte Carlo iterations to converge, a sufficient number of RPV realizations must be evaluated such that there is little change in that quantity with additional RPV realizations. These Monte Carlo iterations are performed by Grizzly in parallel to accelerate these computations, which can be very computationally expensive.

3.2 Methodology for Computational Fluid Dynamics and Transfer

CFD is a powerful tool that allows for geometry and flow conditions to be considered directly in evaluating their effect on the cooling of the RPV wall during thermal shock events. For this study, NekRS, the graphics processing unit-based spectral element CFD code, is used to perform simulations to predict detailed 3D flow patterns that cannot be predicted properly with 1D codes. The temperature is coupled to MOOSE using Cardinal to compute the thermal response of the RPV. An initial effort to simulate RPV-relevant geometries

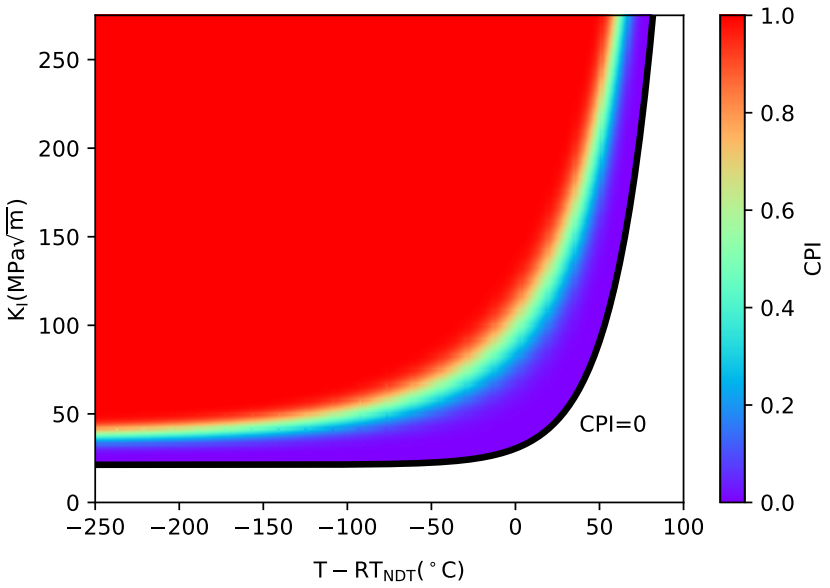

Figure 1: Conditional probability of fracture initiation (CPI) as a function of relative temperature and K_I (from [1]).

during the prior fiscal year is documented in Reference [15], and the models used in the current effort are documented in Reference [16].

While the fluid velocities are important for accurately capturing their effects on the RPV thermal response, the only quantities of interest for the Grizzly PFM simulation are the RPV temperatures. Because the RPV experiences minimal deformation, its mechanical response would only have minimal effect on the CFD model, so a one-way transfer of temperatures from the Cardinal model to the Grizzly model is appropriate here and significantly simplifies the simulation process compared to full two-way coupling.

While it would be possible to directly use the full thermal solution from Cardinal in the Grizzly model, we opted here to transfer only the inner-wall temperatures to Grizzly and use those as Dirichlet boundary conditions used in a thermal model solved in a tightly-coupled manner with the Grizzly mechanical model. This approach allows Cardinal to use a mesh for the RPV wall that is relatively coarse but still adequate to capture the interaction in the thermal response between the RPV wall and coolant, while Grizzly uses a highly refined mesh near the RPV inner surface to accurately capture the thermal gradients that are important for fracture mechanics calculations.

MOOSE has a capability for reading spatially and temporally varying solutions from another finite-element simulation and using those for a variety of purposes through the `SolutionUserObject` and `SolutionFunction` objects. These allow the value of the previous solution to be interpolated at any point in space and time, provided that point is contained within the source finite-element mesh. This approach generally works quite well, except that, when the source and target meshes on curved boundaries do not exactly align, sometimes points in the target mesh lie slightly outside the source mesh. While the solution from the source mesh could be spatially extrapolated to the desired point, it is not necessarily obvious how to do this, so the code simply generates an error in such situations.

This issue with transfers between nonmatching curved meshes was encountered in the present effort, but a solution that works well for this type of problem was developed. A special Dirichlet boundary condition, known as `FunctionOffsetDirichletBC`, was developed that queries a MOOSE `Function` to obtain its

values but applies a small offset in the opposite direction to the surface normal to determine the location where function values are evaluated. This ensures that, with an appropriate offset value, all points on the surface of the receiving model can obtain values from slightly within the domain of the source model.

4 CASE STUDIES

To demonstrate the ability to use the CFD results for spatially varying temperatures in PFM simulations, the same RPV was modeled under two different sets of conditions. Aside from the CFD models and corresponding temperature and pressure conditions applied to the PFM models, all details of these models are identical and are described in Section 4.1. The first case study, described in Section 4.2, made multiple simplifying assumptions in the CFD model and resulted in relatively rapid cooling of the RPV wall. The second case study is a more realistic representation of a small-break loss-of-coolant accident (SBLOCA) and is described in detail in Section 4.3.

4.1 Model Details

All features of the RPV modeled in the two case studies are identical except for loading conditions. The RPV considered here is based on that of a prototypical four-loop pressurized-water reactor (PWR). Figure 2 shows the models for the RPV used by Cardinal and Grizzly. The Cardinal model represented the RPV wall using the finite-element mesh shown, which captures the RPV from the region below the core, where the cylindrical section transitions to a hemisphere, to the region above the inlet and outlet nozzles. Only the RPV wall portion of the Cardinal model is shown here, but there is also a fluid domain that includes the inlet pipe and region between the RPV inner wall and downcomer. Because the RPV region adjacent to the reactor core is most susceptible to fracture (due to the high neutron fluences experienced there), the Grizzly model only represents the core-barrel region, which is a cylinder with a uniform thickness and radius that extends a sufficient distance above and below the core to capture the relevant behavior.

The RPV inner radius is 2.1971 m; it has a 4.064 mm layer of stainless-steel cladding lining the inner surface and total wall thickness of 0.2192 m, including the base metal and liner. The height of the cylindrical core barrel modeled with Grizzly is 4.1 m. A quadrant of the RPV was represented in both the Cardinal and Grizzly models for the global RPV response, with appropriate symmetry conditions. Because of the layout of the inlets and outlets in a typical four-loop PWR, quarter-symmetry conditions are adequate to capture the thermal and mechanical behavior.

Appropriate temperature-dependent thermal and mechanical properties, which include thermal conductivity, specific heat, elastic modulus, Poisson's ratio, and thermal expansion coefficient, were defined for the cladding and base metal. The inner surface wall temperatures from the CFD model are prescribed as boundary conditions on the Grizzly thermomechanical model using the methods described in the previous subsection. The through-wall temperature fields from the Grizzly core-barrel model were verified to compare favorably with those computed by the Cardinal model.

The needed level of mesh refinement to adequately capture gradients in the solution was carefully considered when creating a mesh for the Grizzly global models. The reduced-order model used in the fracture calculations requires a polynomial fit of the stresses through the thickness of the vessel wall, so results can be quite sensitive to mesh refinement. The mesh used in the global analysis for both case studies is shown in Figure 3. This mesh consists of 10 elements in the base metal biased towards the inner surface, along with two equal length elements in the cladding. Both models use second-order, 27-noded hexahedral elements. A convergence study was performed using a 1D global RPV model to determine the appropriate mesh and time stepping for this analysis. The mesh used was determined to be refined sufficiently to provide accurate stress results without significant computational costs.

In this study, an exposure of 40 effective full power years was assumed for the embrittlement model. The spatial distribution of the neutron fluence used in calculating steel embrittlement was obtained from

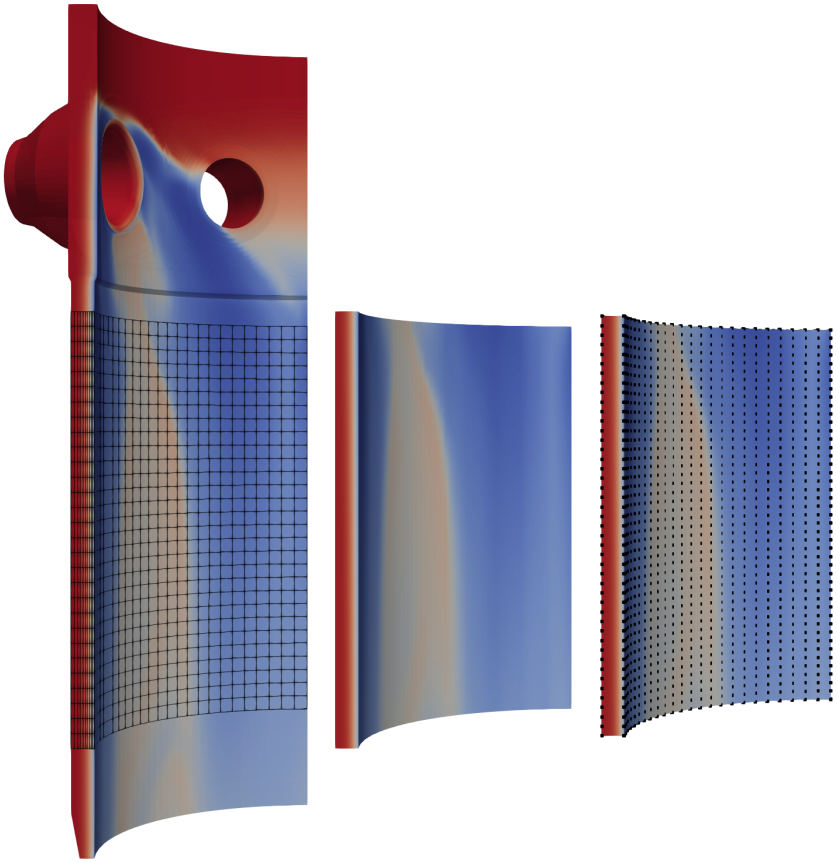

Figure 2: RPV wall models used in this work, showing representative temperature solution field and data flow: (left) Cardinal model of RPV wall with Grizzly mesh of RPV core barrel region superimposed, (center) Grizzly model of core-barrel region, (right) Grizzly model of core-barrel region, showing the endpoints of the lines used to sample data for the PFM model.

field values computed using a coupling of the Virtual Environment for Reactor Applications (VERA) with the Shift radiation transport code [17] and mapped onto a 3D finite-element mesh of the core-barrel region. This fluence map, which was developed for a previous study [10], is used here for demonstration purposes, but is not necessarily tied to this particular transient or RPV design. The fluence distribution is shown in Figure 4 and was originally computed by Shift for 441 effective full power days before being extrapolated to 40 effective full power years.

To capture the variations of the through-wall temperature and stress as a function of axial and azimuthal position in the PFM model, a grid of through-wall sampling points was defined on the global RPV model. This grid of sampling points spans the vessel wall throughout the belt region, and the sampled data is used in fitting polynomial approximations of the through-wall stress and temperature at each grid point. Each flaw sampled in the PFM model uses this data to calculate the SIF using the reduced-order model described in Section 3.1. The grid of line samplers used in these studies is shown as a set of points superimposed on the finite-element model in Figure 2.

Although quarter symmetry is used in the global RPV models, the PFM models capture the population of flaws around the full 360° beltline region of the RPV. Parameters for flaw densities and size and orientation distributions of flaws are were generated by the VFLAW code [18] and used in FAVOR example models, and

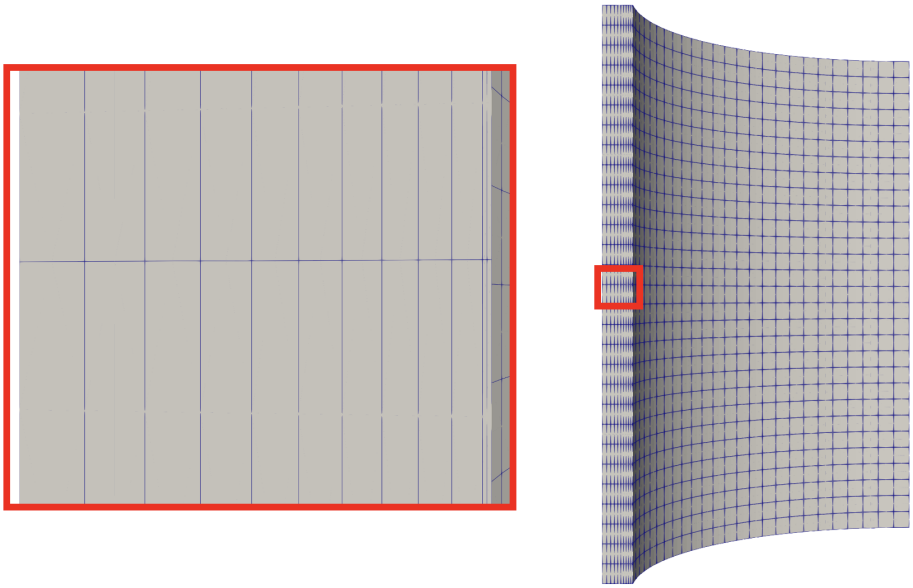

Figure 3: Mesh used in the Grizzly global analysis, showing (left) a detailed view of the through-wall discretization and (right) the full 3D mesh of the quadrant of the core barrel modeled.

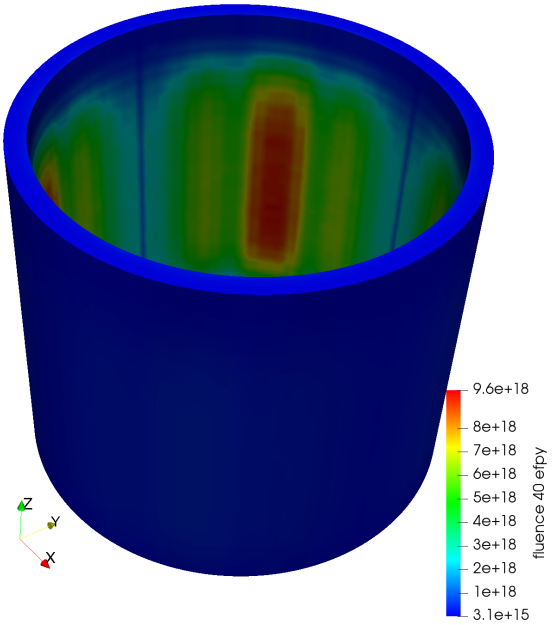

Figure 4: Fluence map computed by Shift and used in case studies, shown in units of neutrons/cm^2 of neutrons >1 MeV extrapolated to 40 effective full power years.

used in prior Grizzly PFM demonstrations [1, 9]. For the present study, only embedded flaws are considered, and no surface-breaking flaws are included in the samples. It is assumed here that the RPV is constructed of ring-shaped forgings connected by circumferential welds. The forgings are assumed to be tall enough that there is only a single circumferential weld at the center of the beltline region, which is assumed to have a height of 3 cm. Material properties for the two PFM models are consistent and representative of actual operating PWRs, which are documented in the Reactor Vessel Integrity Database [19]. To fully characterize the regions that make up the RPV, it is necessary to define the mean values of concentrations of alloying elements and the initial value of RT_{NDT}. Table 1 shows the values of these parameters used in all of these models for the various region types. As with other aspects of this model, these values do not represent the properties of a specific RPV but are typical of those observed in the U.S. reactor fleet.

Table 1: Mean values of key material properties used for the region types in demonstration RPV simulations.

Material	**Cu (wt%)**	**Ni (wt%)**	**Mn (wt%)**	**P (wt%)**	**Initial RT_{NDT} (°F)**
Forging	0.13	0.7	1.44	0.01	50
Weld	0.13	0.1	1.44	0.01	-20

4.2 Proof-of-Concept Scenario

To provide an initial test case for the code-coupling strategy, an initial CFD analysis was performed using multiple simplifying assumptions that resulted in faster run times and in more rapid cooling than would realistically be expected under those conditions. The results of the Grizzly model that used these CFD results are shown here. It is important to emphasize that this is only a proof of concept and does not represent conditions that are actually expected in a realistic accident.

In this proof-of-concept case, the CFD model used flow conditions from an SBLOCA, using laminar flow assumptions and an unrealistically high thermal conductivity in the coolant water. Both of these assumptions were made to obtain significant spatial variations in the RPV wall temperatures in the core-barrel region of the RPV with minimal computational effort. While the results of the model with these assumptions do not represent true thermal-hydraulic conditions within the RPV, this test case demonstrates the spatial variation in the cooling and its effect on the integrity of the vessel. The temperature and through wall stresses are shown in Figure 5 at 300 s in the simulation, and indicate significant axial and azimuthal variations in the temperature and stress fields. In this test case, no internal pressure was applied to the thermomechanical Grizzly model, so all stresses are caused by thermal gradients.

During execution of the model with spatially-varying temperatures shown in Figure 5, the average temperature of the inner wall was computed and saved at each time step. The resulting average surface temperature history was used as an input for a second model that assumes spatially uniform temperatures on the inner RPV surface. Figure 6 shows the average temperature as well as the minimum temperature in the core-barrel region for this scenario. This spatially uniform case highlights the difference between the results computed using spatially varying temperatures and those assuming spatially uniform coolant temperatures.

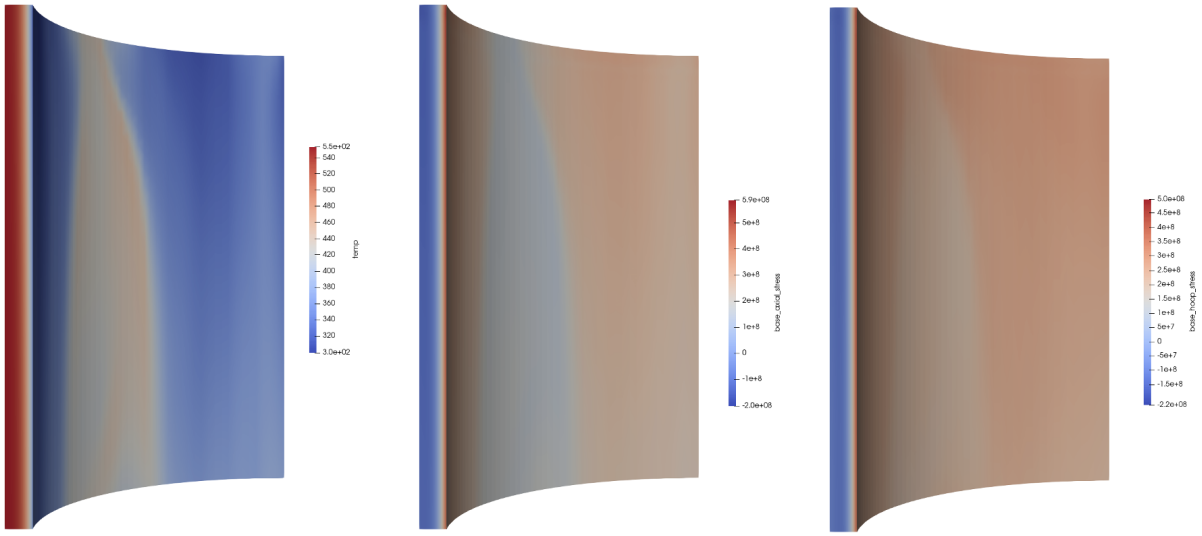

Figure 5: Solution fields predicted by the Grizzly core-barrel model 300 s into the proof-of-concept simulation, with (left) temperature, (center) axial stress, (right) hoop stress shown.

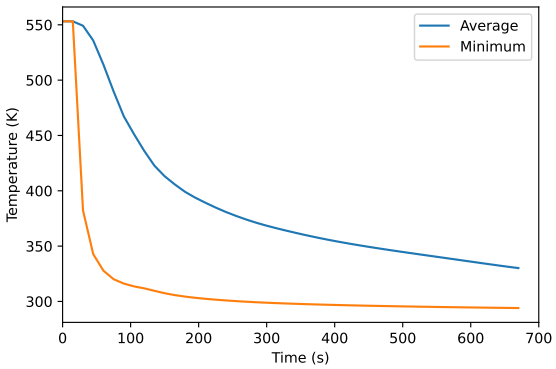

Figure 6: Time histories of spatially averaged and minimum temperature on the inner RPV wall temperature in the core-barrel region model for the proof-of-concept scenario.

PFM models were run based on both the spatially varying and spatially uniform cases. The overall CPI was computed from these models, as well as flaw-specific data for each of the flaws with nonzero CPI values. 50,000 RPV realizations from the Monte Carlo sampling were run, which was adequate for CPI convergence. The CPI convergence plots for the two models are shown in Figure 7. For the spatially uniform case, the final converged average CPI was 7.5×10^{-4}. The model that accounted for nonuniform cooling due to plume effects had a converged average CPI of 2.9×10^{-3}, which is approximately 3.4× higher than the uniform case.

Examining the spatial distribution of the randomly sampled flaws that contributed most to the overall CPI shows that these more critical flaws tend to be located in regions where the cold plume more rapidly cooled the RPV wall. All the flaws in the 90° quadrant of the quarter-symmetry model with nonzero CPI after

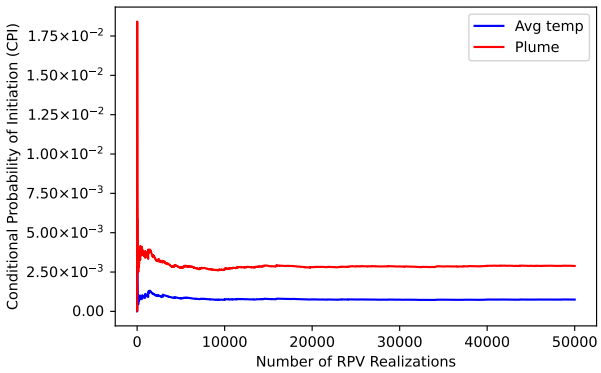

Figure 7: Histories of average CPI, showing convergence over the course of the Monte Carlo iterations for the spatially uniform ("Avg temp") and spatially varying ("Plume") conditions simulated in the proof of concept case study.

50,000 Monte Carlo iterations of the RPV are shown superimposed on the RPV global model in Figure 8, which shows that flaws in the regions cooled at a higher rate have a higher CPI than those in other regions. This plot also shows how critical flaws tend to be clustered more at the middle of the beltline, where fluence is higher, and also shows a concentrated band of critical flaws around the circumferential weld.

Figure 9 shows the spatial distributions of the critical flaws over a quadrant of the RPV for the proof-of-concept PFM models run assuming spatially uniform and nonuniform temperatures. As for Figure 8, these plots show only the flaws with a nonzero CPI for 50,000 RPV samples, but in these plots, the flaws are shown as points colored by their CPI. For both the uniform and nonuniform cooling cases, the concentration of critical flaws on the beltline circumferential weld is evident. For the uniform cooling case, the effects of the nonuniform fluence distribution are visible in the axial and azimuthal variations in the critical flaw concentrations. For the nonuniform cooling case, the effects of more rapid cooling in the regions affected by the cold plume are very pronounced and appear to be more significant than the effects of azimuthal variation in the fluence.

Although this proof-of-concept study employs CFD results that are not representative of actual reactor transient behavior, it highlights how Grizzly and Cardinal can be used to capture the effects of nonuniform cooling and how, under the right conditions, cold-plume effects can have a significant impact on the results of PFM predictions. This scenario has very rapid cooling, so the effects of nonuniform cooling on predicted fracture are likely more pronounced than they would be in more realistic scenarios.

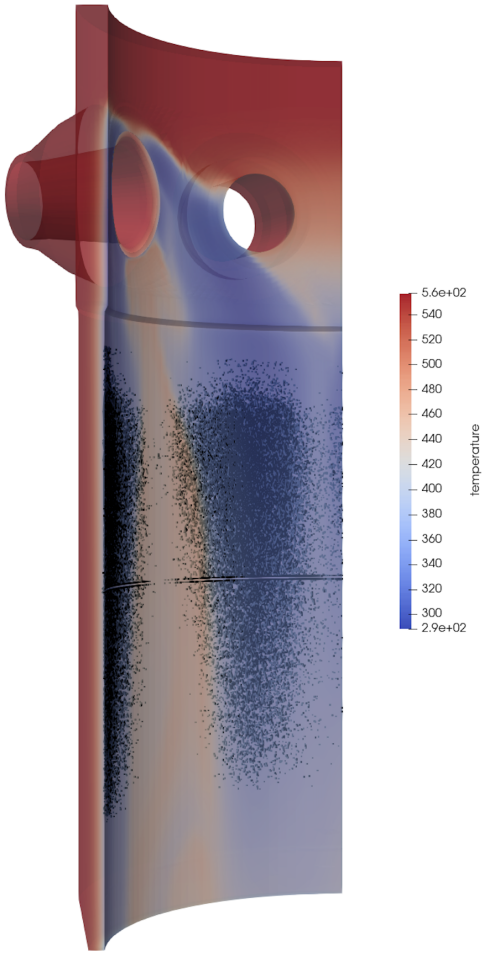

Figure 8: Scatter plot of flaws with nonzero CPI from 50,000 RPV realizations overlaid on the Cardinal-predicted thermal solution 300 s into the transient.

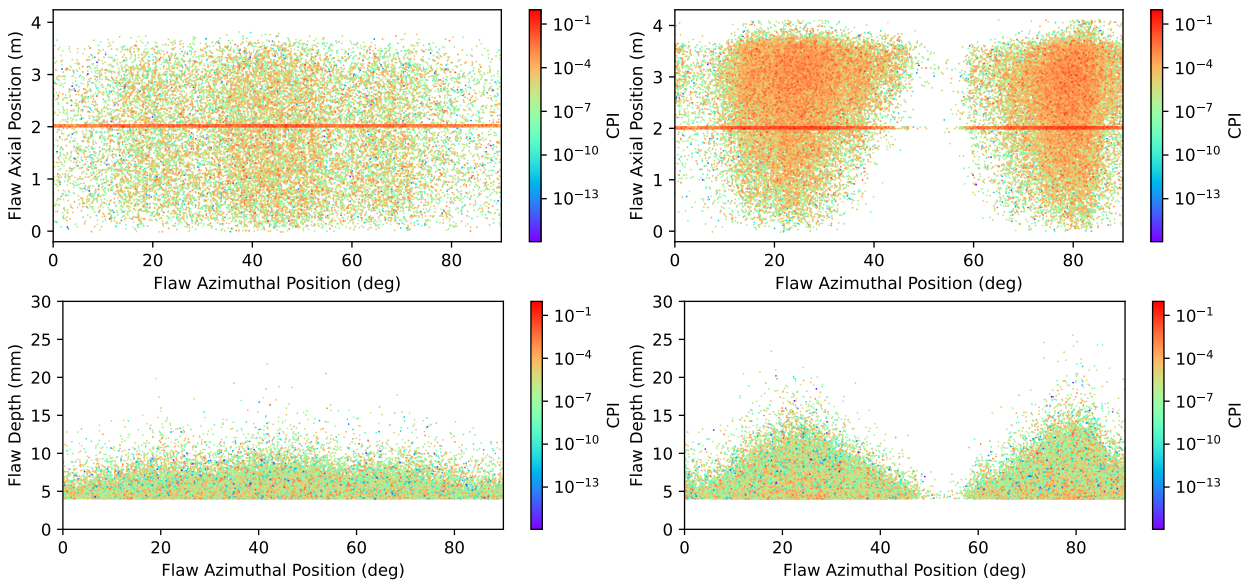

Figure 9: Spatial distributions of flaws with nonzero CPI from 50,000 RPV realizations for the (left) average surface temperature model and (right) cold plume model. Flaw locations are shown in terms of (top) their axial vs. azimuthal positions and (bottom) their depth vs. azimuthal positions.

4.3 Realistic Small-Break Loss-of-Coolant Accident

The same PFM model used in the previous section was also applied to a realistic SBLOCA scenario. For this case study, the boundary conditions for the CFD model mimic those for the SBLOCA case simulated by Reference [6]. A turbulent flow model was employed for the realistic SBLOCA scenario, as were realistic thermal properties of the coolant water. This resulted in much slower cooling of the RPV inner surface, as shown in Figure 10. As for the previous case, temperatures were prescribed on the RPV inner wall based on the Cardinal model. The pressure history shown in Figure 10, which was obtained directly from Figure 4 of Reference [6], was applied to the Grizzly thermomechanical model. Both uniform and nonuniform surface temperature cases were run for this scenario.

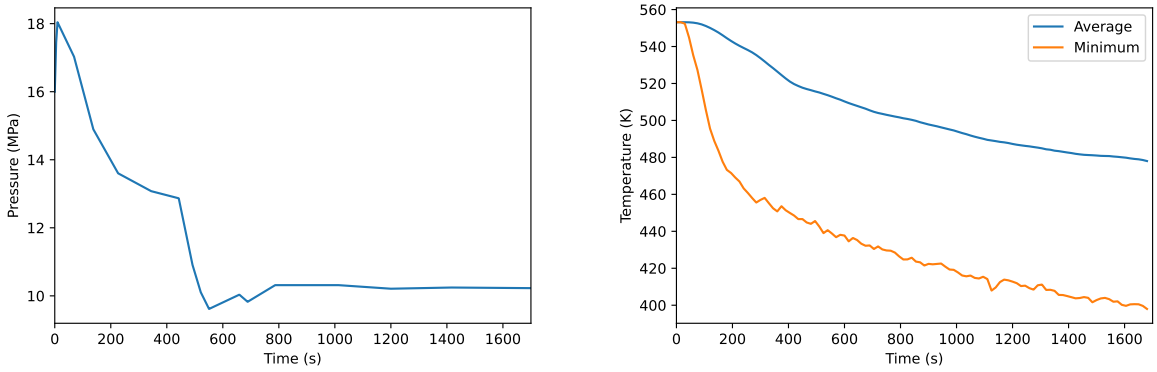

Figure 10: Time histories of (left) pressure and (right) temperature for the realistic SBLOCA scenario. Temperatures are shown both as spatially averaged values on the inner-wall surface as well as the minimum value on the inner wall in the core-barrel region modeled by Grizzly.

Figure 11 shows the temperature fields from the Grizzly thermomechanical model at multiple times during the transient. From these plots, as well as the temperature time histories in it is evident that the cooling is significantly slower than that in the proof-of-concept scenario. After a period of more rapid cooling for approximately the first 300 s, the cooling rate slows down. There is still a pronounced cold plume region, even at the end of the portion of the transient modeled here at 1,680 s.

Unlike the proof-of-concept scenario, this test case had no sampled flaws with CPI > 0, even after a large number of RPV realizations, so the overall CPI = 0 for both the uniform and nonuniform cases. This is a plausible result, because the Weibull probability distribution has no tail on the lower end, so if K_I for a flaw never exceeds the lower-bound toughness curve for its relative temperature, it will never indicate a nonzero CPI.

Because none of the flaws had nonzero CPI values, the types of flaw distribution plots shown in Section 4.2 would not show any flaws. However, the effects of the nonuniform temperatures from the plumes can still be seen in other flaw distribution plots. An alternative metric for flaw severity termed "fracture margin," denoted as m_f, is used here, where:

$$m_f = \frac{K_{IC} - K_I}{K_{IC}} \tag{4}$$

This indicates the fractional margin against exceeding the lower-bound value from the fracture toughness curve at a given temperature, where K_I is the current mode-I SIF and K_{IC} is the mode-I fracture toughness, which is affected by the current temperature, initial toughness, and embrittlement. This fracture margin decreases from 1 to 0 as K_I increases from 0 to K_{IC}, and a negative margin indicates that the lower-bound

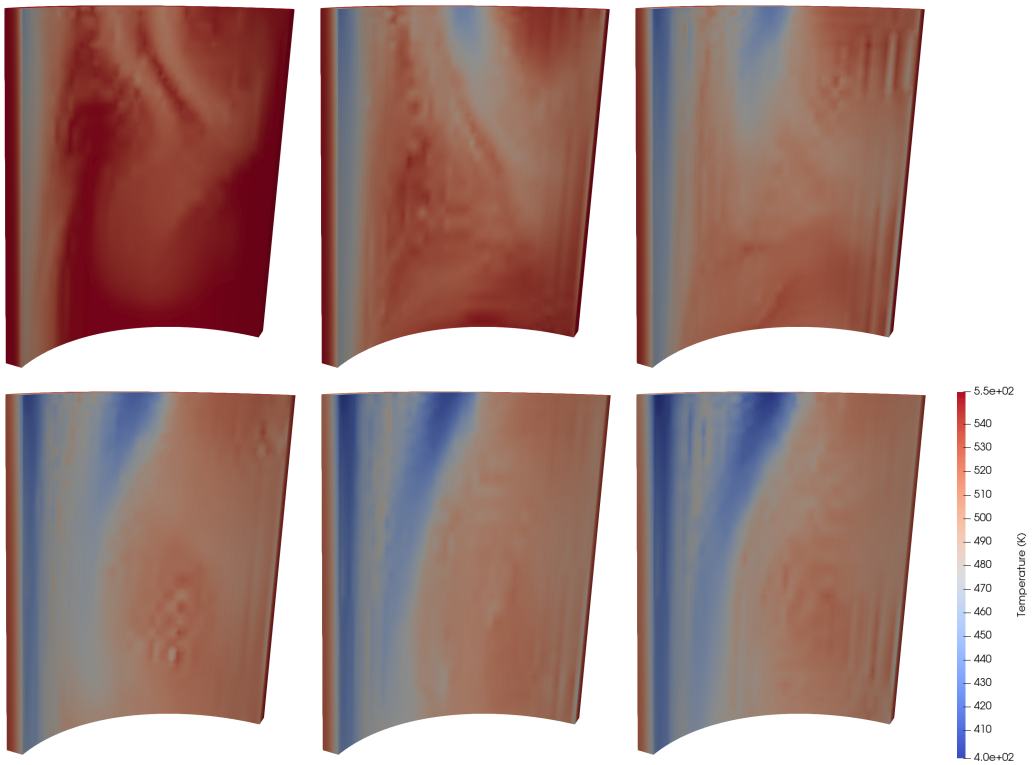

Figure 11: Temperature fields from Grizzly thermomechanical model at times (left to right, top to bottom) 300, 600, 900, 1,200, 1,500, and 1,680 s into the SBLOCA transient.

toughness curve has been exceeded. Note that this metric is based entirely on the fracture toughness curve for the ductile-brittle transition region, with no upper-shelf limit.

Figure 12 shows the 3D distribution of all flaws sampled in the RPV under the SBLOCA scenario from 50 RPV realizations. These flaws are colored based on the minimum value of the fracture margin. The background color has intentionally been made dark in this plot to highlight the fact that the cold-plume-affected regions tend to have flaws with a lower fracture margin. The differences between these regions are rather subtle in this plot. This figure also shows a higher-density band of flaws around the circumferential weld.

Figure 13 shows spatial distributions of flaws with minimum fracture margins below 0.998, colored based on their minimum fracture margin. Although the effects of the plume are less pronounced than they were for the proof-of-concept case, it is evident that regions with more rapid cooling tend to have higher concentrations of more critical flaws. It is important to emphasize, however, that for this scenario the margins against fracture are all very high and even the flaws identified here as being the most critical are quite far away from the potential failure regime.

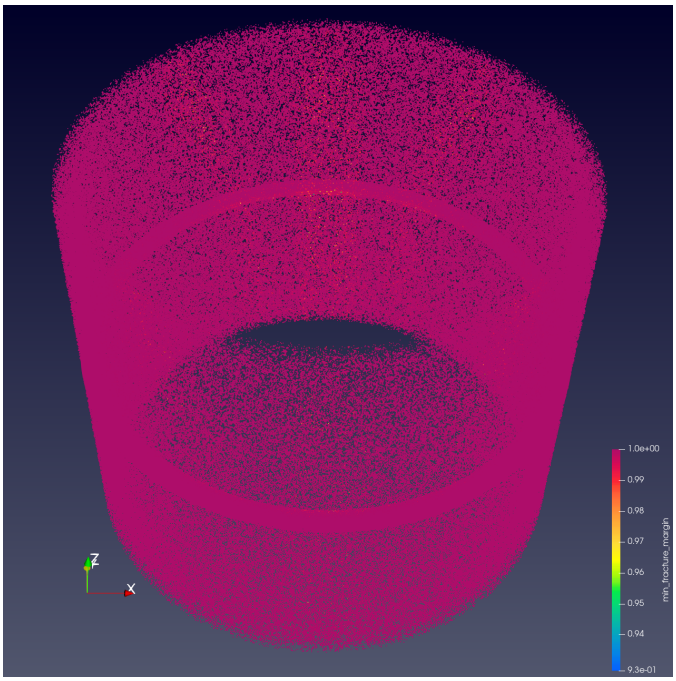

Figure 12: 3D distribution of all flaws from 50 RPV realizations for the SBLOCA scenario with spatially varying temperature, with flaws colored by the minimum value of the fracture margin over the transient.

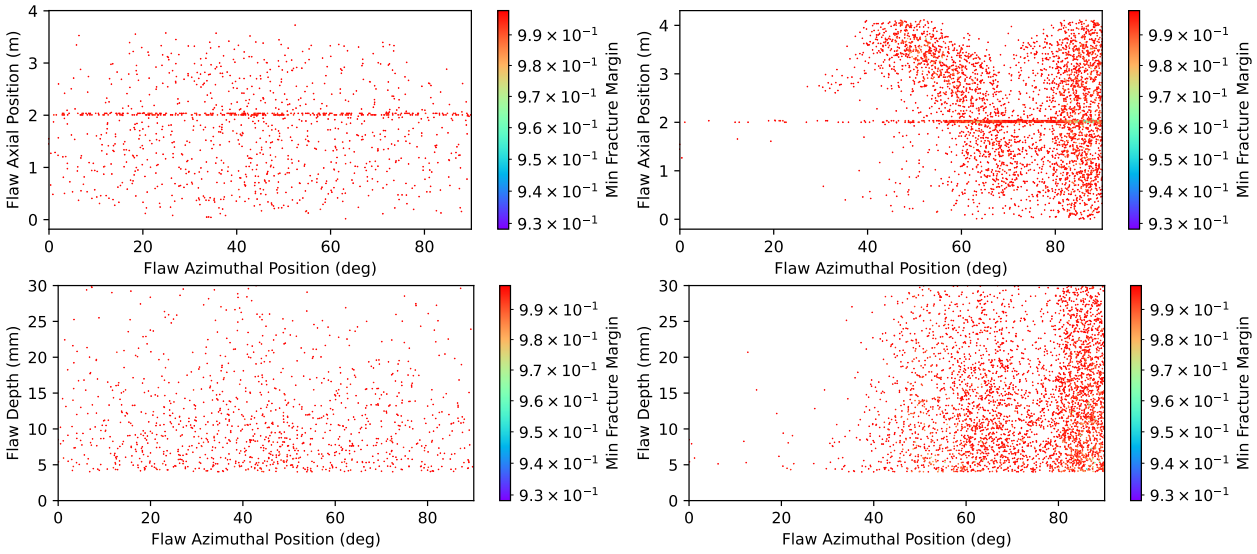

Figure 13: Spatial distributions of flaws with minimum fracture margins below 0.998, from 50 RPV realizations for the (left) average surface temperature model and (right) cold plume model. Flaw locations are shown in terms of (top) their axial vs. azimuthal positions and (bottom) their depth vs. azimuthal positions.

To better illustrate how far the flaws are from the failure regime for this scenario, plots of all the sampled flaws are shown in terms of their K_I and relative temperature values at the time when they reached the minimum fracture margin in Figure 14. Trajectories of the five most critical flaws are shown for the two

models of this scenario. From these plots, it is evident that, in this transient, the relative temperatures for the most critical flaws are still roughly 100 °C higher than the temperature required for fractures.

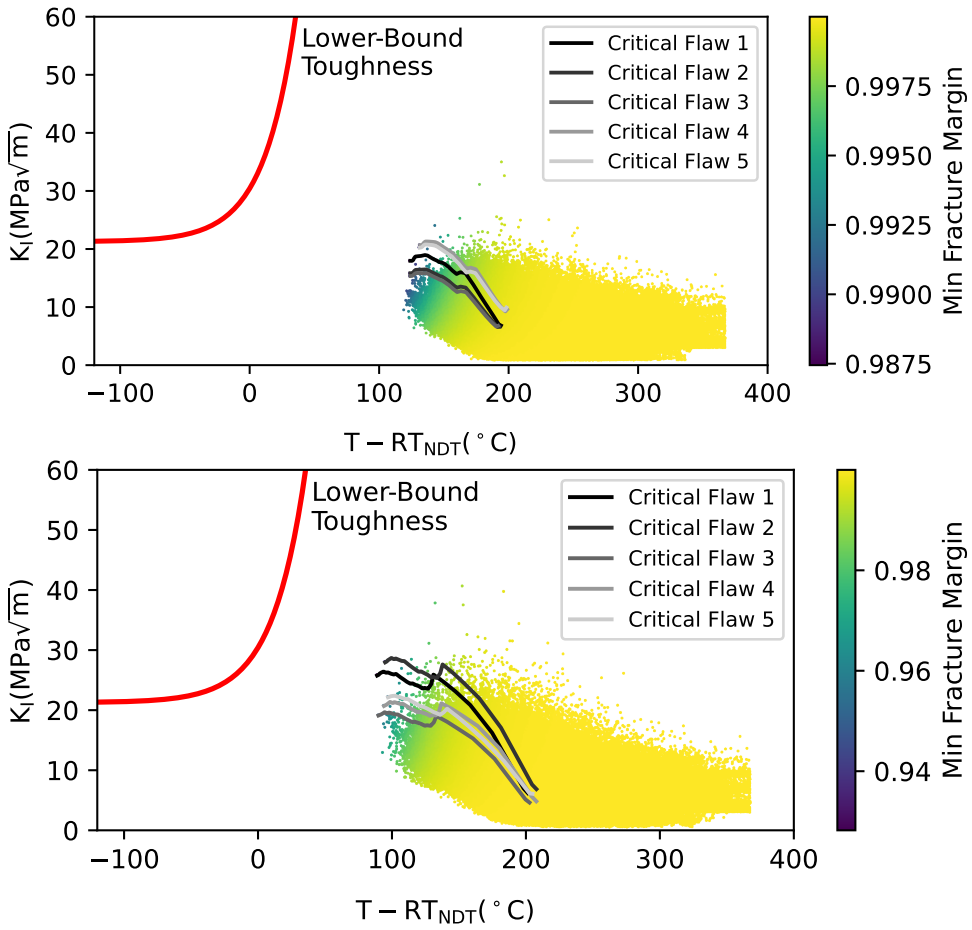

Figure 14: Scatter plot of the K_I and relative temperature values for all sampled flaws from 50 RPV realizations at the point where the fracture margin was at a minimum during the SBLOCA transient. Results are shown for (top) the spatially uniform and (bottom) the nonuniform temperature case. Trajectories of the five most critical flaws are shown for each case.

From the trajectories of the critical flaws in Figure 14, it appears that if the transient were continued further in time, the temperature would likely continue to decrease, leading to a higher likelihood of fracture. However, it also appears that K_I would also decrease, making fracture less likely. It is also important to note that the spatially nonuniform case that accounts for the cold-plume effects does show more flaws with lower relative temperatures, and thus a higher likelihood of fracture, than the spatially uniform case.

While the SBLOCA scenario does not challenge the RPV, and shows significant margins against fracture, it still illustrates how explicitly accounting for the cold-plume effect by using spatially varying temperatures from the CFD model can have a noticeable impact on the predictions of fracture in the sampled populations of flaws. A more severe transient that predicts CPI > 0 would likely indicate higher probabilities of fracture due to the cold-plume effect.

5 SUMMARY AND FUTURE WORK

This report describes a methodology for transferring spatially varying temperature fields for the inner surface of the RPV from high-fidelity CFD simulations to PFM simulations in Grizzly and demonstrates this with two case studies. This enables a first-of-its kind capability to perform PFM on full randomly sampled flaw populations, which is essential for evaluating the significance of cold-plume effects on RPV integrity.

Two case studies were considered here—a proof-of-concept scenario with rapid cooling and a realistic SBLOCA scenario with much slower cooling. The proof-of-concept scenario clearly showed how incorporating spatially nonuniform cooling could have a significant impact on the probability of fracture initiation, with flaws with a higher likelihood of fracture clustered in the more rapidly cooled regions of the RPV. While the realistic SBLOCA scenario did not challenge the RPV's integrity enough to see differences in the predicted probability of fracture, it was still evident that it showed decreased margins against fracture. Further work simulating more aggressive transient conditions is needed to determine whether cold-plume effects are important for realistic LOCA conditions with larger breaks.

In addition to taking into account spatial variations in the RPV wall temperature, the case studies considered here also included spatially varying fluences, which were taken from 3D neutron transport simulations. The alignment of the cold plume, the regions with high fluence, and the welds could potentially have important effects. The tools demonstrated here could readily be used to investigate the effects of the alignment of those features, which is a logical next step for such efforts.

While the methods for transferring solutions from Cardinal CFD models to Grizzly were applied exclusively to LWR RPVs here, these methods are equally applicable for evaluating phenomena of interest for other reactor types. For instance, the effects of thermal striping could be important in high-temperature reactors cooled by molten salt. Models have been developed for crack growth in alloys subjected to these high temperatures [20]. With further development, this type of solution transfer method could be used to evaluate the potential for fatigue crack growth under high-temperature conditions in advanced reactors.

REFERENCES

[1] B.W. Spencer, W.M. Hoffman, and M.A. Backman. Modular system for probabilistic fracture mechanics analysis of embrittled reactor pressure vessels in the Grizzly code. *Nuclear Engineering and Design*, 341:25–37, January 2019. ISSN 00295493. doi: 10.1016/j.nucengdes.2018.10.015.

[2] Naoki Soneda, editor. *Irradiation embrittlement of reactor pressure vessels (RPVs) in nuclear power plants*. Number 26 in Woodhead publishing series in energy. Woodhead Publishing, Waltham, MA, 2015. ISBN 9781845699673. doi: 10.1016/B978-1-84569-967-3.50013-1.

[3] Guian Qian and Markus Niffenegger. Procedures, methods and computer codes for the probabilistic assessment of reactor pressure vessels subjected to pressurized thermal shocks. *Nuclear Engineering and Design*, 258:35–50, May 2013. ISSN 00295493. doi: 10.1016/j.nucengdes.2013.01.030. URL http://linkinghub.elsevier.com/retrieve/pii/S0029549313000587.

[4] Kunio Onizawa, Hiroyuki Nishikawa, and Hiroto Itoh. Development of probabilistic fracture mechanics analysis codes for reactor pressure vessels and piping considering welding residual stress. *International Journal of Pressure Vessels and Piping*, 87(1):2–10, January 2010. ISSN 03080161. doi: 10.1016/j.ijpvp.2009.11.011.

[5] P.T. Williams, T.L. Dickson, B. R. Bass, and H. B. Klasky. Fracture Analysis of Vessels – Oak Ridge, FAVOR, v16.1, computer code: Theory and implementation of algorithms, methods, and correlations. Technical Report ORNL/LTR-2016/309, Oak Ridge National Laboratory, Oak Ridge, TN, September 2016.

[6] V.F. González-Albuixech, G. Qian, M. Sharabi, M. Niffenegger, B. Niceno, and N. Lafferty. Integrity analysis of a reactor pressure vessel subjected to a realistic pressurized thermal shock considering the cooling plume and constraint effects. *Engineering Fracture Mechanics*, 162:201–217, August 2016. doi: 10.1016/j.engfracmech.2016.05.010.

[7] Guian Qian, Markus Niffenegger, Medhat Sharabi, and Nathan Lafferty. Effect of non-uniform reactor cooling on fracture and constraint of a reactor pressure vessel. *Fatigue & Fracture of Engineering Materials & Structures*, March 2018. ISSN 8756758X. doi: 10.1111/ffe.12796.

[8] H.J. Uitslag-Doolaard, L. Stefanini, A. Shams, and F.J. Blom. Numerical prediction of a single phase Pressurized Thermal Shock scenario for crack assessment in an Reactor Pressure Vessel wall. *Annals of Nuclear Energy*, 144:107563, September 2020. ISSN 03064549. doi: 10.1016/j.anucene.2020.107563.

[9] Benjamin W. Spencer, William M. Hoffman, Sudipta Biswas, Wen Jiang, Alain Giorla, and Marie A. Backman. Grizzly and BlackBear: Structural component aging simulation codes. *Nuclear Technology*, 207(7):981–1003, April 2021. doi: 10.1080/00295450.2020.1868278.

[10] Benjamin W. Spencer, William M. Hoffman, Benjamin S. Collins, and Shane C. Henderson. Coupling of neutron transport and probabilistic fracture mechanics codes for analysis of embrittled reactor pressure vessels. In *ASME Pressure Vessels and Piping Conference*, pages PVP2020–21680, Virtual, Online, August 2020. American Society of Mechanical Engineers.

[11] E.D. Eason, G.R. Odette, R.K. Nanstad, and T. Yamamoto. A physically-based correlation of irradiation-induced transition temperature shifts for RPV steels. *Journal of Nuclear Materials*, 433(1-3):240–254, February 2013.

[12] H. F. Bückner. A novel principle for the computation of stress intensity factors. *Z. angew Math. Mech.*, 50:529–546, 1970.

[13] *ASME Boiler and Pressure Vessel Code, Section XI, Rules for Inservice Inspection of Nuclear Power Plant Components*. Number ASME BPVC.XI-2017. ASME, 2017.

[14] R. C. Cipolla. Computational method to perform the flaw evaluation procedure as specified in the asme code, section xi, appendix a. Technical Report EPRI Report NP-1181, Failure Analysis Associates, September 1979.

[15] Yiqi Yu, April Novak, Dillon Shaver, and Elia Merzari. Multi physics simulation on reactor pressure vessel (RPV) subjected to pressurized thermal shock (PTS). Technical Report ANL/NSE-22/30, Argonne National Laboratory, May 2022.

[16] Yiqi Yu, Dillon Shaver, and Elia Merzari. Simulation and analysis on reactor pressure vessel (RPV) subjected to pressurized thermal shock (PTS) under SBLOCA scenario by using Cardinal to support the fracture mechanics analyses. Technical Report ANL/NSE-23/76, Argonne National Laboratory, 2023.

[17] Tara Pandya, Katherine Royston, Eva Davidson, Tom Evans, Andrew Godfrey, Shane Henderson, Cole Gentry, Shane Stimpson, and Benjamin Collins. High-fidelity ex-core capabilities in VERA. *EPJ Web of Conferences*, 247:06024, 2021. doi: 10.1051/epjconf/202124706024. URL `https://doi.org/10.1051%2Fepjconf%2F202124706024`.

[18] F. A. Simonen, S. R. Doctor, G. J. Schuster, and P. G. Heasler. A generalized procedure for generating flaw-related inputs for the FAVOR code. Technical Report NUREG/CR-6817, PNNL-14268, Pacific Northwest National Laboratory, Richland, WA, March 2004. URL `http://www.nrc.gov/docs/ML0408/ML040830499.pdf`.

[19] US Nuclear Regulatory Commission. Reactor vessel integrity database version 2.0.1 (RVID 2), July 2000. URL `https://www.nrc.gov/reactors/operating/ops-experience/reactor-vessel-integrity/database-overview.html`.

[20] Antonio Recuero, Markian Petkov, Benjamin W. Spencer, and Pierre-Alexandre Juan. Continuum damage mechanics modeling of high-temperature flaw propagation: Application to creep crack growth in 316H standardized specimens and nuclear reactor components. *Journal of Pressure Vessel Technology*, pages 1–26, July 2023. doi: 10.1115/1.4062953.